Bulletin of Mathematical Biology (2002) **64**, 829–860
doi:10.1006/bulm.2002.0303
Available online at http://www.idealibrary.com on

A Two-Variable Model of Somatic–Dendritic Interactions in a Bursting Neuron

CARLO R. LAING AND ANDRÉ LONGTIN
Department of Physics,
University of Ottawa,
150 Louis Pasteur,
Ottawa, ON,
Canada, K1N 6N5
E-mail: claing@science.uottawa.ca

We present a two-variable delay-differential-equation model of a pyramidal cell from the electrosensory lateral line lobe of a weakly electric fish that is capable of burst discharge. It is a simplification of a six-dimensional ordinary differential equation model for such a cell whose bifurcation structure has been analyzed (Doiron *et al*., *J. Comput. Neurosci.*, **12**, 2002). We have modeled the effects of back-propagating action potentials by a delay, and use an integrate-and-fire mechanism for action potential generation. The simplicity of the model presented here allows one to explicitly derive a two-dimensional map for successive interspike intervals, and to analytically investigate the effects of time-dependent forcing on such a model neuron. Some of the effects discussed include 'burst excitability', the creation of resonance tongues under periodic forcing, and stochastic resonance. We also investigate the effects of changing the parameters of the model.

1. INTRODUCTION

Bursting, in which a cell periodically switches from quiescent behavior to a rapidly spiking state and back again, from quiescent behavior to a

Recently, a new mechanism for burst discharge in pyramidal cells of the weakly electric fish *Apteronotus leptorhynchus* was investigated (Doiron *et al*., 2002). These cells receive input directly from electroreceptor cells on the fish's skin, and are thought to play a significant role in the processing of electrosensory information. The model presented in Doiron *et al*. (2002) was a set of six coupled nonlinear first-order ordinary differential equations, which was a reduction from the multicompartment model involving over 1500 variables presented in Doiron *et al*. (2001a). This reduction was obtained by lumping the many compartments into two, representing the soma and the dendrite, and by ignoring the dynamics of the channels not thought to be important in the mechanism for bursting. That the model in Doiron *et al*. (2002) reproduced both the bursting behavior observed in the model of Doiron *et al*. (2001a) and experimentally observed bursts (Lemon and Turner, 2000) indicates that this process was successful.

The model analyzed in Doiron *et al*. (2002) was studied using the 'slow–fast' approach of others (Rinzel and Ermentrout, 1998; Izhikevich, 2000), but it differed from all previous bursting models in that when the one slow variable was held constant, the remaining 'fast' system did not show bistability for any values of the slow variable. The bifurcation in the fast system that ended a burst was found to be a transition from period-one to period-two behavior associated with the failure of a somatic action potential to induce a dendritic one, and the interburst interval was found to involve the passage in phase space near a fixed point. Several aspects of the timing of bursts were found to be related to the distance in parameter space from a saddle–node bifurcation, hence the name 'ghostbursting' (Strogatz, 1994).

In this paper we further reduce the model in Doiron *et al*. (2002) to a set of two discontinuous delay differential equations, from which a two-dimensional map can be derived (assuming constant input current). This gives us analytical insight into complex soma–dendrite interactions, and is computationally much easier to study than an ODE model. The reduced model presented here can be constructed because, as a result of the work in Doiron *et al*. (2002), we understand the essential ingredients of this type of bursting (refer to Fig. 1). A short time after most somatic spikes, current flows from the dendrite to the soma, producing a depolarizing afterpotential (DAP) at the soma. For large enough current injected to the soma, the sizes of these DAPs slowly increase due to a slow inactivation of the dendritic potassium that is responsible for the repolarization of dendritic action potentials. This results in progressively smaller inter-spike intervals (ISIs), and this process continues until an ISI is smaller than the refractory period of the dendrite. Once this happens, there is dendritic spike failure, which removes the normal current flow to the soma, and a DAP does not appear. This results in a long ISI, during which the variable controlling inactivation of dendritic potassium increases, and the sequence starts again. In Fig. 1 we show typical bursting behavior from the model in Doiron *et al*. (2002). The spike patterning is similar to that seen in the multicompartment model in Doiron *et al*. (2001a) and in experimental recordings (Lemon and Turner, 2000).

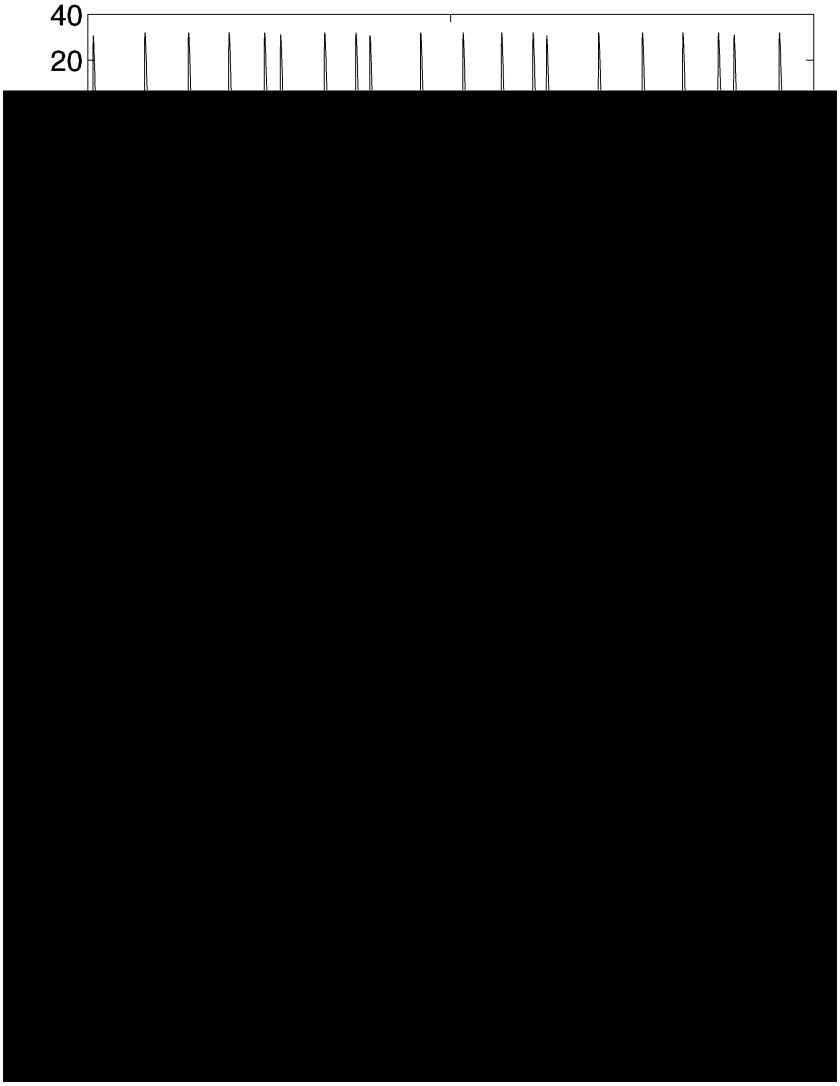

Figure 1. An example of bursting for the 6-variable ODE model of Doiron *et al*. (2002). Top: somatic voltage, middle: dendritic voltage, bottom: dendritic potassium inactivation. Bursts terminate at t approximately 75, 90, 115 and 140. middlnlF74 8.96p2sium inactivation.

In this paper we also consider periodically modulating the current applied to the model neuron, and for the case of sinusoidal modulation we obtain a three-dimensional map for successive spike times. This map can be used to determine the boundaries in parameter space of resonance tongues, in which the neuron's firing frequency is locked to that of the forcing. This map is able to explain some of the behavior seen in Laing (2002), in which bursting models [including the one in Doiron *et al*. (2002)] are periodically forced. For example, when only a DC current is injected into the model neuron (Doiron *et al*. 2002), there is a value of current at which the neuron switches from tonic to bursting behavior. However, adding a sinusoidal modulation to the injected current can either increase or decrease the DC

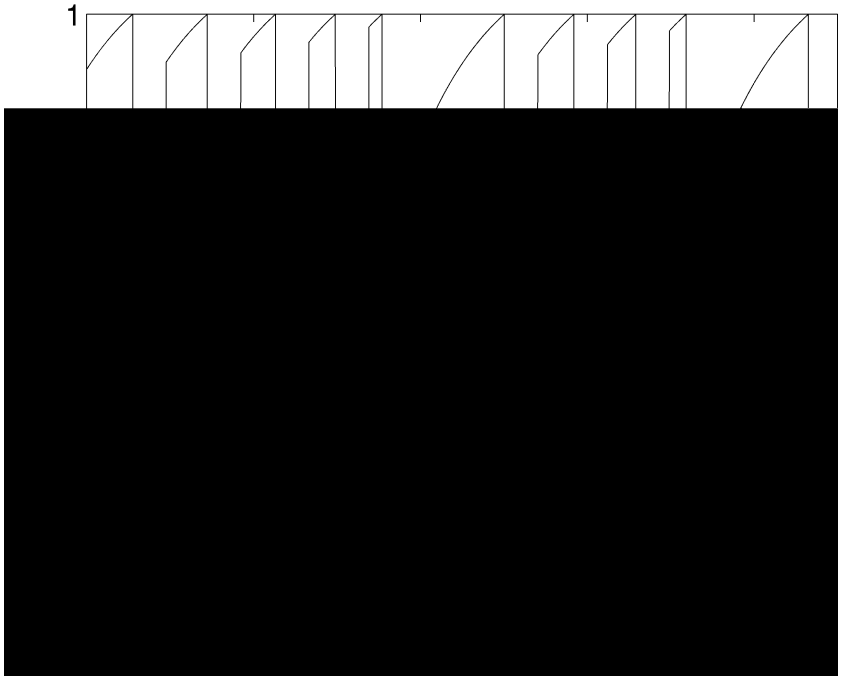

Figure 2. Voltage (top) and c (bottom), the variable representing the amount of feedback from the dendrite to the soma, as functions of time, illustrating the bursting behavior of (1), (2). Parameters are $I = 1.3$, $A = 2.3$, $B = 0.15$, $C = 2$, $r = 0.7$, $\sigma = 0.4$, $\tau = 1$.

models for other types of neurons, provided the interactions between the soma and dendrites are understood.

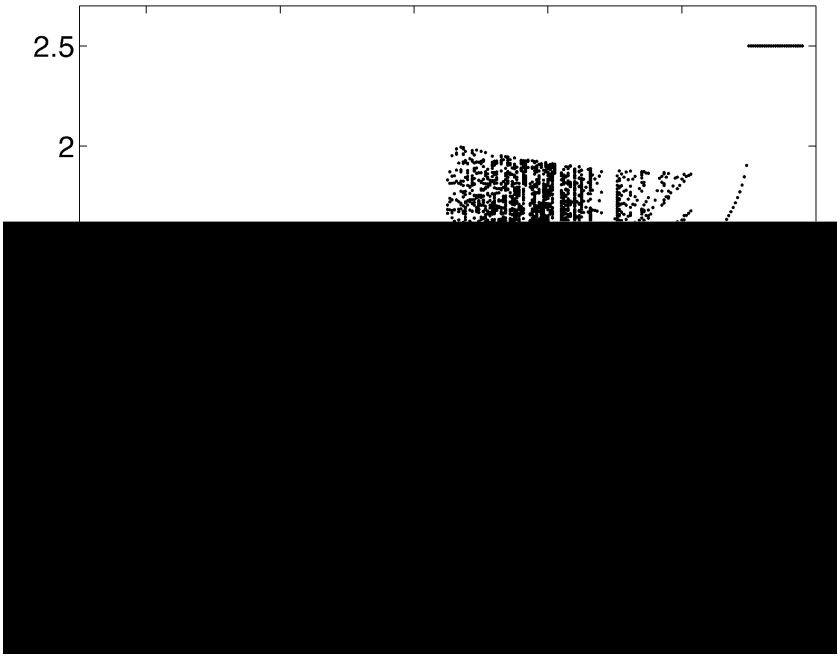

Figure 3. Instantaneous frequency (reciprocal of ISI) as a function of input current, I, for the map (7), (8

$_{n+1}$ in this situation may cause the values of c_i to increase without bound, an unphysical situation. Note that we must have $\sigma < r$.

The instantaneous frequency, i.e., $1/\ _n$, is shown as a function of I in Fig. 3 for a particular set of parameter values (transients have been removed). A number of observations can be made:

1. During periodic firing for $1 < I <\square 1.22$, case *(ii)* in (7) will always be true. For periodic firing, $c_{n+1} = c_n$, and thus (8) is a quadratic in c_n. It can therefore be solved for c_n in terms of the steady-state period, (the negative square root must be chosen). Substituting this into case *(ii)* in (7), we obtain an equation that must satisfy:

$$(1 - I)e^{-\sigma}e \quad = \frac{Ae^{-\sigma/\tau}\left[1 - e^{-\ /\tau} - \sqrt{1 - 2e^{-\ /\tau} + (1 - 4BC)e^{-2\ /\tau}}\right]}{2Ce^{-2\ /\tau}}$$

$$- Ie^{-\sigma}. \tag{9}$$

   For $1 < I <\square 1.22$, equation (9) has two solutions, the larger one of which is stable (and can be seen in Fig. 3; the unstable solution is not shown). The two solutions coalesce in a saddle–node bifurcation (Kuznetsov, 1995) at $I \square 1.22$. Note that in (1), (2), this is a saddle–node bifurcation of periodic orbits. Interestingly, it was a saddle–node bifurcation of periodic orbits that separated periodic from bursting behavior in the full ionic ODE model in Doiron *et al*. (2002). As $I \to 1$ from above, the largest root of (9) tends to ∞, corresponding to the frequency tending to zero. Note that if $\tau = 1$, (9) is independent of σ.
2. For I greater than $\square 1.22$, the smallest instantaneous frequency occurs between bursts, where the only current driving the neuron during its entire period is I. Thus the lower curve in Fig. 3 for I greater than $\square 1.22$ is just $= \ln[I/(I - 1)]$ [case *(iii)* in (7)].
3. For I greater than $\square 1.22$, the 'band' of frequencies in Fig. 3 not including the interburst interval is bounded below by the curve

$$= \sigma + \ln\left[\frac{ABe^{-\sigma/\tau} - Ie^{-\sigma}}{1 - I}\right] \tag{10}$$

   since c_n has a minimum value of B after being reset at the end of the interburst interval. [Expression (10) is obtained by setting $c_n = B$ in (7) *(ii)*

In relation to point 1 earlier, if the positive square root is taken instead and substituted into case *(ii)* in (7), the roots of the resulting function may not satisfy the condition $\quad > r$ associated with case *(ii)*, and thus they will not be actual fixed points of the map. Also, the fact that (8) can be solved explicitly for the steady-state value of c is a result of our choice of the dynamics of c, (2). Replacing the term Cc^2 in (2) by Cc would mean that the equation for the steady state of c was linear and thus had only one solution; this choice would also simplify the expression (9), but would make chaotic behavior more difficult, although not impossible, to obtain (see later).

2.2. ***Lyapunov exponent.*** The Lyapunov exponents of a trajectory determine its stability and the behavior of nearby trajectories. If a stable solution has at least one positive Lyapunov exponent, the system will exhibit sensitivity to initial conditions, and nearby trajectories will typically separate exponentially in time (Drazin, 1992). For a range of current values, the bursting behavior in Doiron *et al*. (2002) was shown to have a positive Lyapunov exponent, and thus be chaotic.

To find the maximal Lyapunov exponent, λ, for a trajectory of the map (7), (8), we analytically calculate the Jacobian, Df, of (7), (8) and evaluate it at each point on the orbit, $x_1, x_2, \ldots$, where $x_i = (\ _i, c_i) \in \mathbf{R}^2$. If q_i is the largest magnitude eigenvalue of $Df(x_i)$ then λ can be calculated (Drazin, 1992) from

$$\lambda = \lim_{n \to \infty} \frac{1}{n} \sum_{i=1}^{n} \ln |q_i|. \tag{11}$$

This quantity is shown in Fig. 4, multiplied by four for clarity, together with instantaneous frequency. Note the transition from period-1 firing to chaotic bursting at $I \approx 1.22$, and the long-period quasiperiodic behavior for I greater than ≈ 1.32.

2.3. ***Effects of parameters.*** The model (1), (2) has six parameters that are regarded as constant (A, r, σ, τ, B and C). We now briefly discuss the effects of changing each of these. In more realistic models (Doiron *et al*., 2001a, 2002), changing parameters can mimic the application of drugs that selectively block various ionic channels [23.55 Td[(channels)-2rlg8;8337 1.636 Td[(j)]TJ/J/F2720B

grow extremely quickly. This leads to 'doublet' firing in V and an eventual breakdown of the algorithm.

- For the parameters used, if $\tau > 1$, increasing σ makes the neuron more likely to burst and vice versa. If $\tau < 1$, increasing σ makes the neuron less likely to burst, and vice versa. This can be understood graphically by writing (9) as

$$e^{-\sigma} f(\ ) = Ae^{-\sigma/\tau} g(\ , \tau) \tag{12}$$

where

$$f(\ ) = I + (1 - I)e \tag{13}$$

and

$$g(\ , \tau) = \frac{1 - e^{-\ /\tau} - \sqrt{1 - 2e^{-\ /\tau} + (1 - 4BC)e^{-2\ /\tau}}}{2Ce^{-2\ /\tau}}. \tag{14}$$

For a given τ and other parameters in the appropriate range, $f(\ )$ is a concave-down function of , and $g(\ , \tau)$ is a concave-up function of . They are both positive in the region of interest. The intersections of the left and right sides of (12) give the values of at the two periodic orbits (one stable and the other unstable) of (1), (2). It is the coalescence of these in a saddle–node bifurcation that marks the transition from periodic to bursting behavior.

If $\tau > 1$, increasing σ decreases the left-hand side of (12) more than it decreases the right-hand side, bringing the two points of intersection closer to one another, and thus lowering the value of I at which the saddle–node bifurcation occurs. Conversely, if $\tau < 1$, increasing σ decreases the right-hand side of (12

without having to simulate those more detailed models. To determine these relationships, one would need to know the effects of changing a particular parameter in a large model on one or more of the six parameters discussed earlier.

As an example, it was found in Doiron *et al*. (2002) that decreasing the maximum conductance of the dendritic potassium decreased the value of current injected to the soma at which the cell switched from tonic to bursting, i.e., it made the cell more likely to burst. This is easy to understand, since it is dendritic potassium that is responsible for repolarizing the dendrite, and by lessening its effect the dendritic

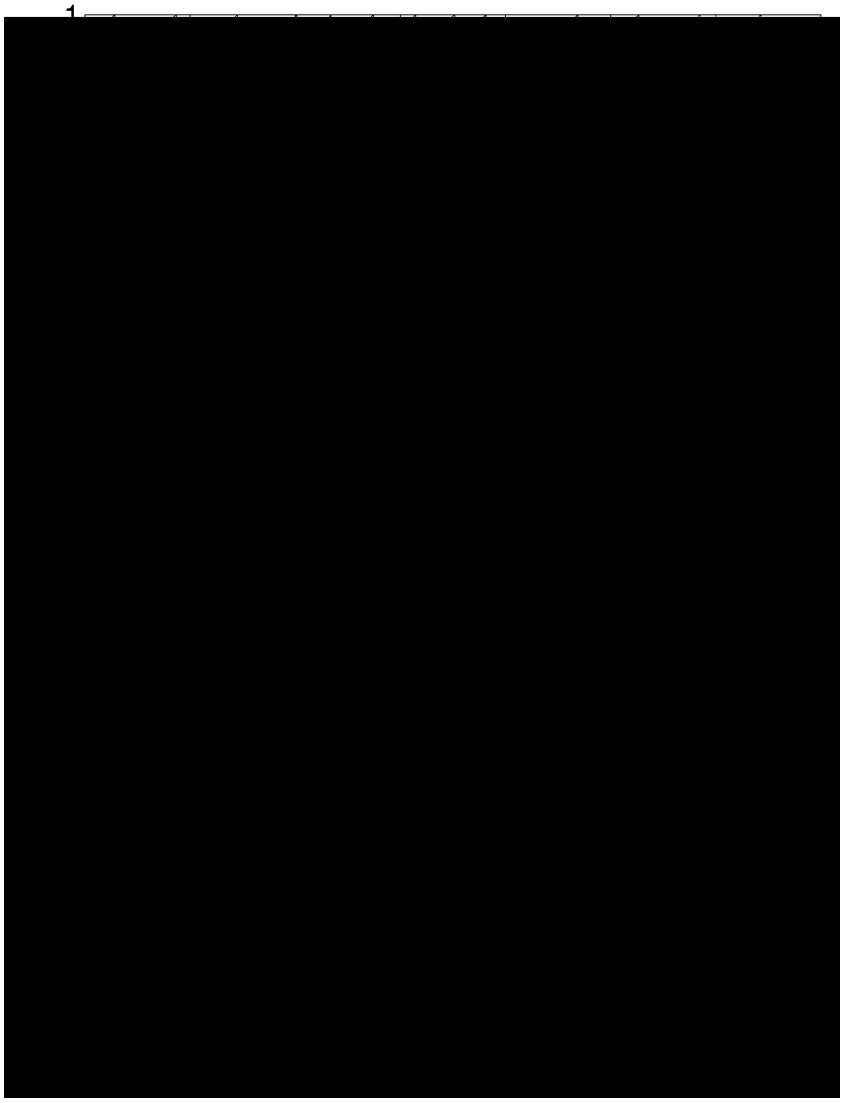

Figure 5. Burst excitability for the system (1), (2). I was set to 1.5 for $4 < t < 4.8$ for the top two panels, and 1.45 for $4 < t < 4.8$ for the bottom two panels. $I = 1.21$ otherwise. In the top two panels a burst is induced, and in the lower two no burst is induced. Note that there is no bistability in the system, and that the slow recovery after the perturbations is due to the system being pushed close to an unstable periodic orbit. Parameters are $A = 2.3$, $B = 0.15$, $C = 2$, $r = 0.6$, $\sigma = 0.4$, $\tau = 1$.

that 'slow' behavior in a bursting system does not necessarily imply the existence of a slow time-scale in the form of an explicit long time-constant, but can be the result of the system's trajectory in phase space passing close to the stable manifold of an unstable object (e.g., a fixed point or periodic orbit).

This form of burst excitability has been seen in the model presented in Doiron *et al*. (2002). Since the pyramidal cells we are modeling receive sensory input

directly from electroreceptors on the fish's skin (Nelson *et al*., 1997; Chacron *et al*., 2001

Figure 6. The curve of saddle–node bifurcations of periodic orbits (solid) and the threshold for firing (dashed), as a function of B. Other parameters are the same as in Fig. 3. The two curves meet at a codimension-two point, marked with a circle. The labels refer to the types of behavior that occur within each region of parameter space.

is within the refractory period of the dendrite, so no DAP arrives after it and a long ISI is produced (long because I is close to 1).

It is possible that the bursts produced by these cells are of most interest, rather than the individual spikes within them (Lisman, 1997). Thus being able to change both the number of spikes in a burst and the length of the interburst interval, as we have just done, may be very important with respect to changing the information content of the output of such a cell (Doiron *et al*., 2002).

One difference between the model (1), (2) and the ODE model of Doiron *et al*. (2002) involves the scaling of the interburst intervals as I decreases. The bifurcation separating quiescence from periodic firing in Doiron *et al*. (2002) is a saddle–node-on-a-circle bifurcation (Kuznetsov, 1995), and hence the period of periodic firing scales as $T \sim 1/\sqrt{I - I^*}$, where I^* is the value of the current at which the transition takes place. This is in contrast with the $= \ln[I/(I-1)]$ expression for the integrate-and-fire mechanism that we are using in (1), (2) to produce action potentials. Thus in the interburst intervals, where there is essentially no current flowing from the dendrite to the soma and the soma is driven by only the current injected into it from the outside, the length of the interburst intervals will scale differently with current for the two models. However, both scalings give the same qualitative result, i.e., $T \to \infty$ as $I \to I^*$ from above, and $\to \infty$ as $I \to 1$ from above. The scaling in (1), (2) could be made to match the scaling in

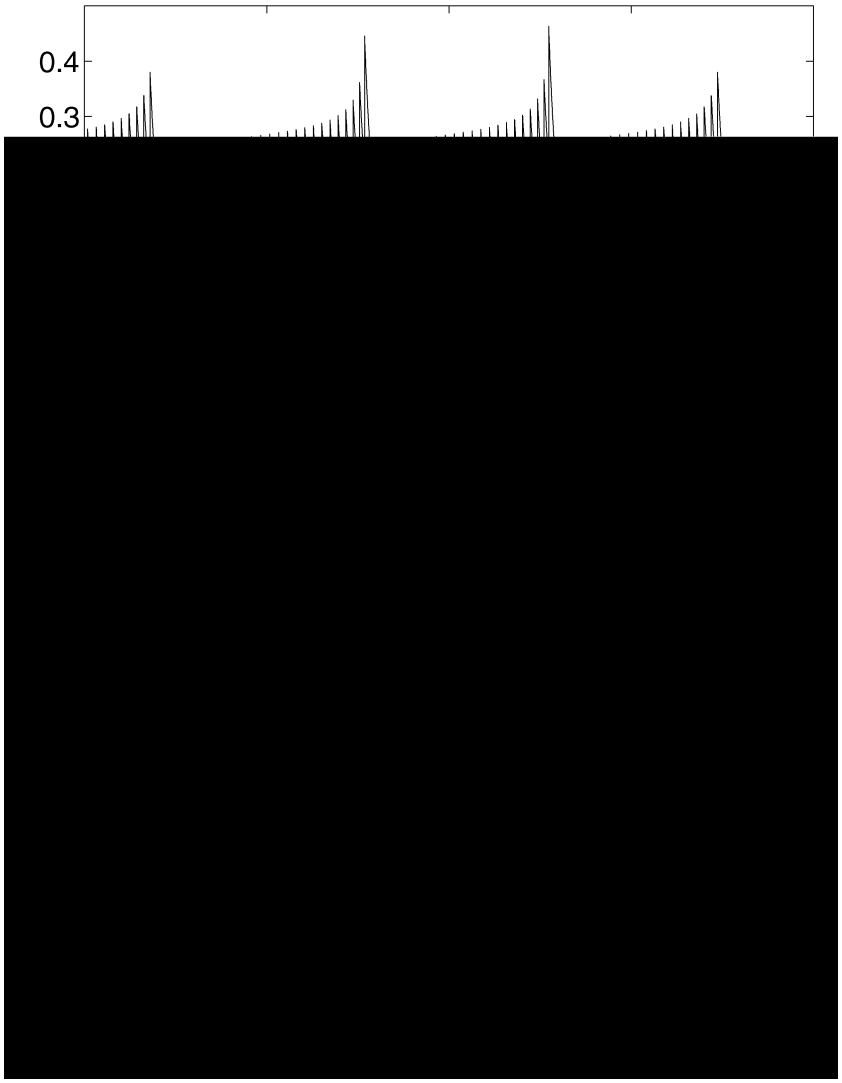

Figure 7. Example bursts of (1), (2) for three different (I, B) pairs. Top: $(I, B) = (1.23, 0.15)$, middle: $(I, B) = (1.007, 0.37)$, bottom: $(I, B) = (1.007, 0.5)$. See Fig. 6. Other parameters are the same as in Fig. 3. Note that the horizontal axes all have the same scale.

Doiron *et al*. (2002) if the spike-producing neuron was one whose bifurcation separating quiescence from periodic firing was a saddle–node-on-a-circle bifurcation; one example is the 'theta neuron' (Gutkin and Ermentrout, 1998), but its nonlinearity would complicate analysis of the resulting bursting model.

3. SINUSOIDAL FORCING

et al. (1981); Glass and Mackey (1988); Glass (1991); Coombes and Bressloff (1999); Smith *et al*. (2000); Coombes *et al*. (2001

we need to solve (16) with $V(t_n + \sigma) = \overline{V} + Ac_n e^{-\sigma/\tau}$. This has the solution

$$V(t; t_n, c_n) = I + \frac{}{1 + \omega^2} [\sin(\omega t) - \omega \cos(\omega t)]$$

$$+ e$$

(Glass, 1991), and are labeled by the ratio of frequencies, e.g., 3 : 2. (For this example, the oscillator would pass through two cycles in the same time that the forcing signal took to pass through three cycles.) The system (1), (2) is capable of periodically oscillating for some values of its parameters and input, so under periodic forcing we expect it to have some features in common with periodically forced oscillators. However, the presence of the bifurcation separating periodic from burst firing in the unforced system may mean that new features appear when it is periodically forced.

Consider the case of $q:1$ locking, where we have one firing during a period of qT ($\omega = 2\pi/T$), i.e., during q forcing cycles. For this case, $c_{n+1} = c_n$, so let c^* be the smallest root of

$$c_n = c_n e^{-qT/\tau} + B + C\left(c_n e^{-qT/\tau}\right)^2. \tag{32}$$

We can see from (20) that in this periodically-locked state

$$1 = I + \frac{}{1+\omega^2}\left[\sin\right.$$

Combining the two terms involving φ_n, equation (36) can be rewritten as

$$1 - I - e^{\sigma - qT}[Ac\,e^{-\sigma/\tau} - Ie^{-\sigma}] = (1 - e^{-qT})\frac{}{\sqrt{1+\omega^2}}\sin(\varphi_n$$

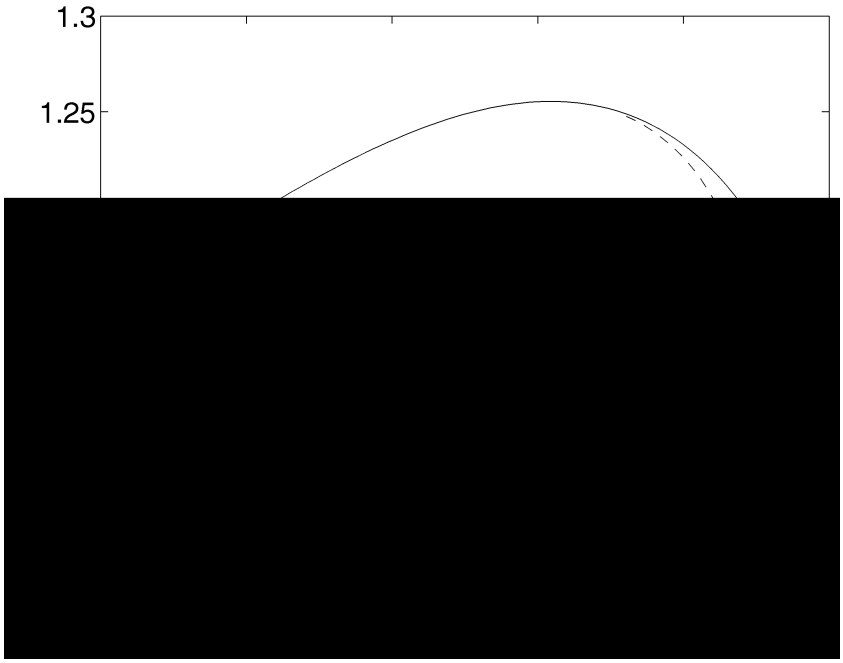

Figure 8. Boundaries of the 1 : 1 tongue from (40) (solid line) for the map (27)–(29). The dashed line indicates the curve of subcritical Hopf bifurcations. = 0.2, other parameters are as in Fig. 3.

solutions was then determined by evaluating the eigenvalues of a numerically-determined approximation of the Jacobian of (27)–(29) at the corresponding points.]

This process of finding the boundaries of resonance tongues can be carried out for other frequency ratios, but the resulting equations are more complicated. Note that this procedure is not affected by the presence of the periodic → bursting boundary in parameter space. A similar observation was made in Yoshino *et al*. (1999), where the authors studied a periodically forced Fitzhugh–Nagumo system as the underlying dynamics changed from excitable to oscillatory. Note also that Fig. 8 is

Figure 9. Bistability for the map (27)–(29) when $I = 1.22$ (cf. Fig. 8). The top panel shows iterates of the map, while the bottom one shows the 1 : 1 locked solution and its stability, for exactly the same parameter values (the 1 : 1 solution loses stability through a subcritical Hopf bifurcation—see text). Note that for $-6.88 < I < -7.08$, there is evidence of bistability, as the attractor in the top panel is not the same as that in the bottom panel. Parameters are as in Fig. 8.

Note that this decrease in threshold could not be predicted from looking at Fig. 8, since the transition into bursting for this value of ω does not involve leaving the 1 : 1 tongue. Thus the effective 'burst threshold' can be either increased or decreased, depending on the frequency of forcing, as was observed in Laing (2002). This phenomenon of shifting the effective threshold has not yet been observed with actual pyramidal cells, but should be straightforward to verify.

3.2. ***Stochastic resonance.*** Stochastic resonance is the phenomenon whereby moderate amounts of noise, when added to a system that has a subthreshold input signal, cause the signal to be observable in the system's output (Gammaitoni *et al*., 1998). For small noise intensities the signal cannot be observed, as it is subthreshold, and for high intensities the system's output is swamped by the noise, so if the signal to noise ratio at the output is plotted as a function of noise intensity, it will show a maximum at some moderate value of noise intensity.

We have already derived a map, (27)–(29), for the sinusoidally forced system (1), (2), and we can use this to show stochastic resonance in (1), (2), since it already incorporates a signal—the sinusoid. One choice of modeling the effect of noise is

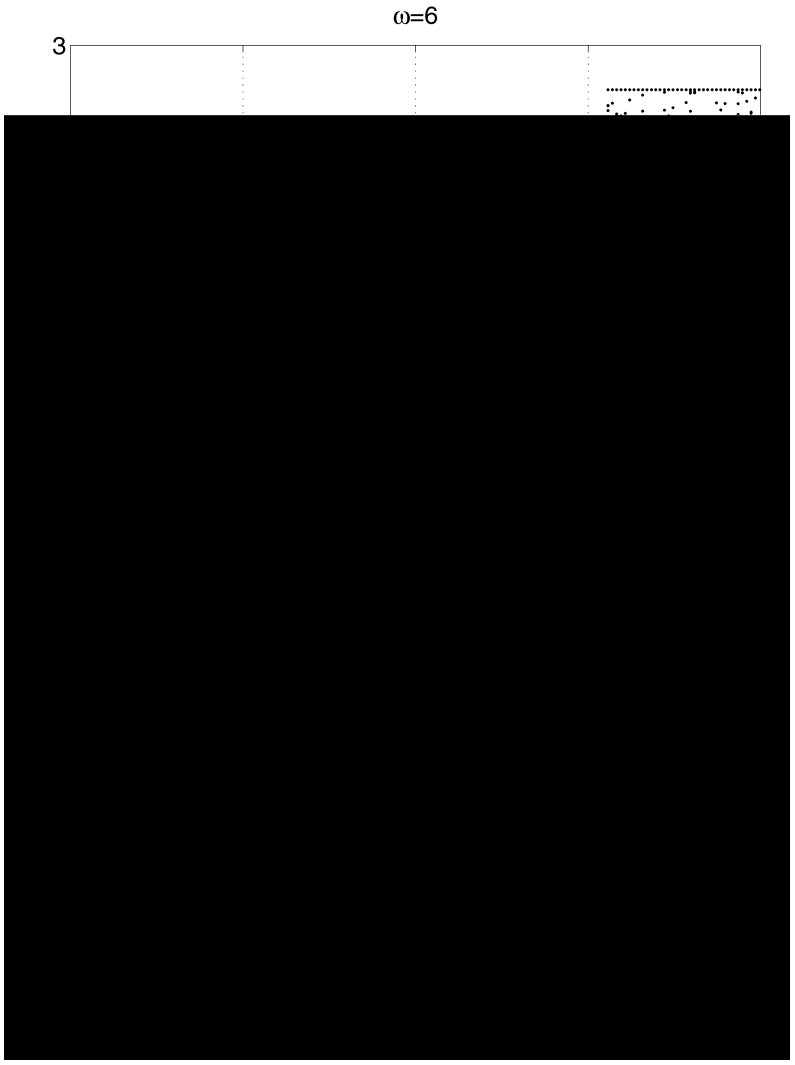

Figure 10. Instantaneous frequency (dots) and the maximal Lyapunov exponent (solid line) as a function of I for $\omega = 6$ (top) and $\omega = 7.15$ (bottom). See Fig. 8. With no periodic forcing the system shows bursts for I greater than □1.22, so depending on the frequency

!

In order to quantify the signal to noise ratio, we need to choose which aspect of the system (1), (2) is to be considered as the output. As was done in Laing (2002), we use the high-frequency 'doublets' that occur at the end of a burst. These could

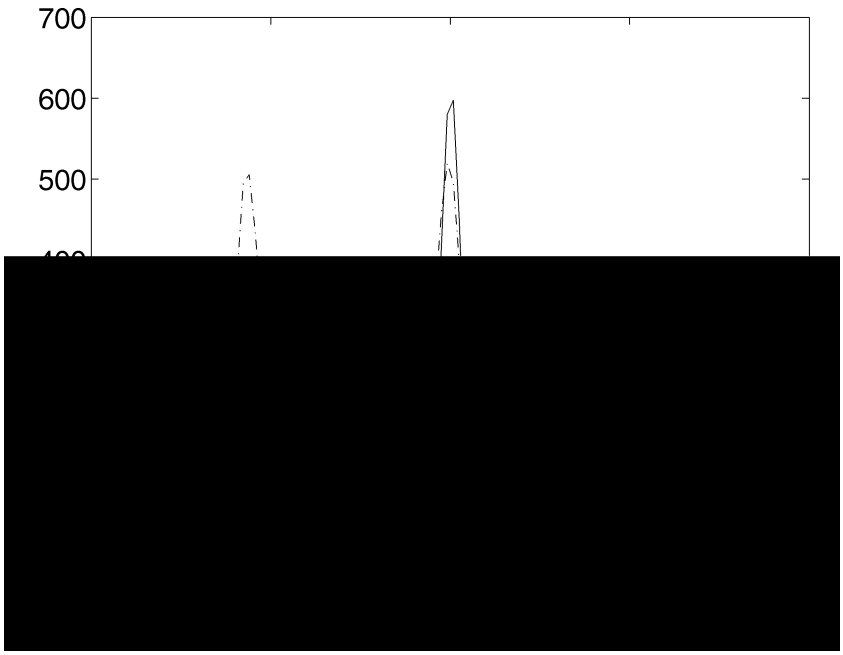

Figure 11. The power spectrum of (27), (28) and (42) as defined in (43)–(45) for $\varepsilon = e^{-6}$ (dashed), $\varepsilon = e^{-4}$ (solid) and $\varepsilon = e^{-2}$ (dash–dotted). Other parameter values are $I = 1.21$, $A = 2.3$, $B = 0.15$, $C = 2$, $\sigma = 0.4$, $\tau = 1$, $r = 0.6$, $\quad = 0.02$, $\omega = 0.1$. The spectra result from averaging over five noise realizations with $N = 3000$. Note that $I = 1.21$ is just below the bifurcation separating periodic from burst firing (see Fig. 3).

a simplification of the six variable ODE model presented in Doiron *et al.* (2002), which was itself a drastic simplification of the multicompartment model of

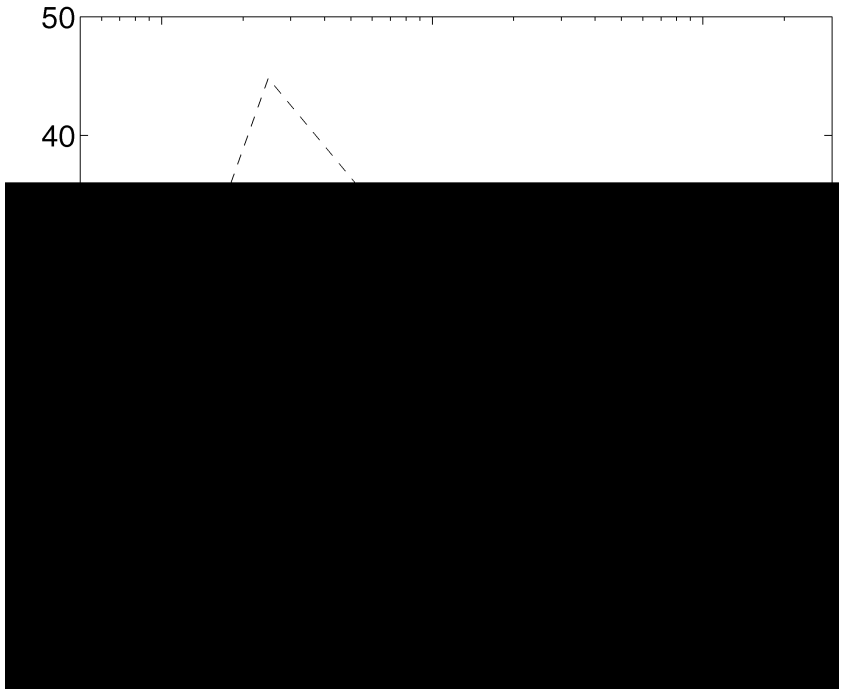

Figure 12. The signal to noise ratio of (27), (28) and (42) as defined in (43)–(45) as a function of ε. Parameters are as in Fig. 11. The dashed lines indicate $\pm$ one standard deviation.

This reduced model is of use because of its simplicity. Computationally it is much simpler to simulate than ionic models, and it also has fewer parameters that can be varied. Because of our understanding of the mechanisms we are modeling (

a dynamic variable, so that it increased during a burst, as is known to occur (Turner, 2002). Then a burst could be terminated by a decreasing ISI meeting an increasing refractory period, resulting in the failure to produce a DAP. Another example could involve including a refractory period in the soma and investigating the effects of

alternative to (1) is

$$\frac{dV}{dt} = I - V + Ac \sum_n H(t_n - t_{n-1} - r)s(t - t_n) \tag{A.2}$$

where

$$s(t) = \frac{ab}{b-a} H(t)(e^{-at} - e^{-bt}), \qquad 0 < a < b \tag{A.3}$$

and the contribution to the term involving s from firings other than the most recent may or may not be taken into account. For (A.2), (A.3), V and its first derivative will be continuous between firings, and the time to the peak of s can be related to the effective delay between a somatic action potential and the maximum flow of current from dendrite to soma. A disadvantage of using these smoother forms of delayed feedback is that even in the unforced case, the map (7), (8) can no longer be written explicitly, but will involve equations that must be solved numerically.

It is also possible to replace the Heaviside function, $H(x)$, that determines whether there is effective feedback from the dendrite to soma in (1) with a smooth approximation, e.g., $[1 + \tanh(\nu x)]/2$, where ν is sufficiently large. Doing this would remove the distinction between cases *(ii)* and *(iii)* in (7). The $B + Cc^2$ term in (2) could also be replaced by an increasing function of c, but this would affect both the analytical tractability of the system and its chaotic nature.

It is also possible to have partial failure of backpropagation, rather than complete. This would involve replacing the Heaviside function in (1) with, for example

$$(1 - \alpha)H(t_n - t_{n-1} - r) + \alpha H(r + t_{n-1} - t_n) \tag{A.4}$$

where α

The modifications presented above may be useful for other applications of the model (1), (2), for example, simulating an array of such neurons, and demonstrate that there is no single 'correct' model of ghostbursting, but rather a variety.

ACKNOWLEDGEMENTS

We thank Maurice Chacron and Brent Doiron for helpful conversations regarding the ideas presented here, and the referees for their very helpful comments. This work was funded by NSERC and a PREA award from the government of Ontario.

REFERENCES

Av-Ron, E., H. Parnas and L. A. Segel (1993). A basic biophysical model for bursting neurons. *Biol. Cybern.* **69**, 87–95.

Booth, V. and A. Bose (2001). Neural mechanisms for generating rate and temporal codes in model CA3 pyramidal cells. *J. Neurophysiol.* **85**, 2432–2445.

Chacron, M. J., A. Longtin and L. Maler (2001). Negative interspike interval correlations increase the neuronal capacity for encoding time-dependent stimuli. *J. Neurosci.* **21**, 5328–5343.

Coombes, S. and P. C. Bressloff (1999). Mode locking and Arnold tongues in integrate-and-fire neural oscillators. *Phys. Rev. E* **60**, 2086–2096.

Coombes, S., M. R. Owen and G. D. Smith (2001). Mode locking in a periodically forced integrate-and-fire-or-burst neuron model. *Phys. Rev. E* **64**, 041914.

de Vries, G. (1998). Multiple bifurcations in a polynomial model of bursting oscillations. *J. Nonlinear Sci.* **8**, 281–316.

Doiron, B., A. Longtin, R. W. Turner and L. Maler (2001a). Model of gamma frequency burst discharge generated by conditional backpropagation. *J. Neurophysiol.* **86**, 1523–1545.

Doiron, referee0(of 1 k (1d

Goldbeter, A. (1996). *Biochemical Oscillations and Cellular Rhythms: The Molecular Bases of Periodic and Chaotic Behaviour*, Cambridge University Press.

Guevara, M. L., L. Glass and A. Shrier (1981). Phase locking, period-doubling bifurcations, and irregular dynamics in periodically stimulated cardiac cells. *Science* **214**, 1350–1353.

Gutkin, B. S. and G. B. Ermentrout (1998). Dynamics of membrane excitability determine interspike interval variability: a link between spike generation mechanism and cortical spike train statistics. *Neural Comput.350–1353.*

Press, W. H., S. A. Teukolsky, W. T. Vetterling and B. P. Flannery (1992). *Numerical Recipes in C*, 2nd edn, Cambridge University Press.

Rinzel, J. and G. B. Ermentrout (1998). Analysis of neural excitability and oscillations, in *Methods in Neuronal Modeling: From Ions to Networks*, C. Koch and I. Segev (Eds), MIT Press.

Rulkov, N. F. (2000). Regularization of synchronized chaotic bursts. *Phys. Rev. Lett.* **86**, 183–186.

Segev, I. and W. Rall (1998). Excitable dendrites and spines: earlier theoretical insights elucidate recent direct observations. *Trends Neurosci.* **21**, 453–460.

Sivan, E., L. Segel and H. Parnas (1995). Modulated excitability: a new way to obtain bursting neurons. *Biol. Cybern.* **72**, 455–461.

Smith, G. D., C. L. Cox, S. M. Sherman and J. Rinzel (2000). Fourier analysis of sinusoidally driven thalamocortical relay neurons and a minimal integrate-and-fire-or-burst model. *J. Neurophysiol.* **83**, 588–610.

Steriade, M., I. Timofeev, N. Dürmüller and F. Grenie (1998). Dynamic properties of corticothalamic neurons and local cortical interneurons generating fast rhythmic (30–40 Hz) spike bursts. *J. Neurophysiol.* **79**, 483–490.

Strogatz, S. H. (1994). *Nonlinear Dynamics and Chaos: With Applications to Physics, Biology, Chemistry, and Engineering*, Reading: Addison-Wesley.

Terman, D. (1992). The transition from bursting to continuous spiking in excitable membrane models. *J. Nonlinear Sci.* **2**, 135–182.

Traub, R. D., M. A. Whittington, I. M. Stanford and J. G. Jefferys (1996). A mechanism for generation of long-range synchronous fast oscillations in the cortex. *Nature* **383**, 621–624.

Turner, R. W. (2002). Personal communication.

Vetter, P., A. Roth and M. Häusser (2001). Propagation of action potentials in dendrites depends on dendritic morphology. *J. Neurophysiol.* **85**, 926–937.

Wang, X.-J. (1993). Genesis of bursting oscillations in the Hindmarsh–Rose model and homoclinicity to a chaotic saddle. *Physica D* **62**, 263–274.

Wang, X.-J. (1999). Fast burst firing and short-term synaptic plasticity: a model of neocortical chattering neurons. *Neuroscience* **89**, 347–362.

Yoshino, K., T. Nomura, K. Pakdaman and S. Sato (1999). Synthetic analysis of periodically stimulated excitable and oscillatory membrane models. *Phys. Rev. E* **59**, 956–969.

Zupanc, G. K. H. and L. Maler (1993). Evoked chirping in the weakly electric fish (*Apteronotus leptorhynchus*): a quantitative biophysical analysis. *Can. J. Zool.* **71**, 2301–2310.

Received 18 November 2001 and accepted 15 April 2002